ACS OMEGA

Open Access

http://pubs.acs.org/journal/acsodf

Article

Modification-specific Proteomic Analysis Reveals Cysteine S-Palmitoylation Involved in Esophageal Cancer Cell Radiation

Qingtao Ni, Chi Pan,* and Gaohua Han*

Cite This: *ACS Omega* 2025, 10, 1541−1550

Read Online

ACCESS | Metrics & More | Article Recommendations | Supporting Information

ABSTRACT: This study aimed to investigate the effects of radiation (RT) on protein and protein S-palmitoylation levels in esophageal cancer (EC) cell lines. EC cells (N = 6) were randomly divided into RT and negative control. The results revealed that 592 proteins were identified in the RT group, including 326 upregulation proteins and 266 downregulation proteins. These differentially expressed proteins were involved in cellular biological processes. S-palmitoylation sequencing analysis revealed that 830 and 899 S-palmitoylation cysteine sites were upregulated and down-regulated, respectively. Differential S-palmitoylation proteins were primarily found in cellular processes, anatomical entities, and binding activities. Kyoto encyclopedia of genes and genomes (KEGG) pathway and protein−protein interaction analysis revealed that differential S-palmitoylation proteins are involved in proteoglycans in cancer, shigellosis, EGFR tyrosine kinase inhibitor resistance, nucleocytoplasmic transport, and mineral absorption. In conclusion, this study demonstrated that RT significantly affects protein expression and S-palmitoylation levels in EC cell lines, which has implications for cancer biology-related cellular processes and pathways. These findings enhance understanding of the molecular mechanisms underlying the response of EC cells to RT treatment.

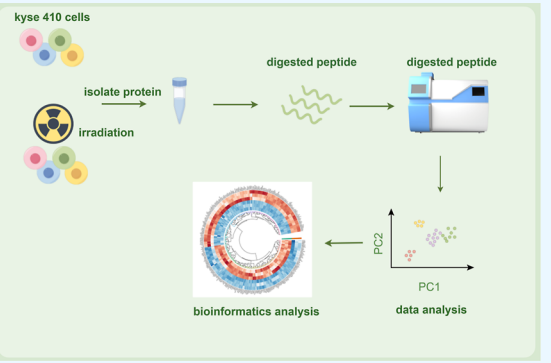

INTRODUCTION

Esophageal cancer (EC) is a malignancy that develops from the epithelial tissue of the esophagus. It has a 5 year survival rate of approximately 20%.[1] Over 50% of all cases of EC originate in China, and the disease is prevalent among disadvantaged populations.[2] EC treatment typically involves a combination of surgery, radiotherapy, and chemotherapy.[3] However, only a small percentage of patients with EC exhibit a complete pathological response to neoadjuvant chemoradiation therapy.[4] Radiation (RT) exposure causes scarring in the heart tissue.[5] Ribosomal S6 protein kinase 4 is essential in promoting cancer stem-like cell properties and radioresistance in EC.[6] The precise mechanisms underlying RT resistance in EC are unclear. However, various factors, including gene mutation, DNA methylation, and histone modification, confer resistance to cancer cells.[7] Nevertheless, a comprehensive and systematic understanding of proteins and protein modifications after EC cell radiotherapy remains unknown.

Proteins and their modifications are essential in cancer development. The context-dependent dynamics of histone modification are essential in gene epigenetic regulation.[8] The hydroxyisobutyrylation of lysine in *N*-acetyltransferase 10 promotes cancer metastasis.[9] The modification of the p53 protein with isoLGs reduces acetylation and modulates p53-dependent gene transcription.[10]

The lipidation modification of proteins is a significant biological phenomenon in which lipid moieties are covalently linked to proteins.[11] S-palmitoylation is the most common of the five recognized types of lipid covalent modifications.[12] This process involves the covalent bonding of a palmitate molecule to a cysteine residue within a protein, thereby exerting regulatory control over its function. Palmitoylation is a significant post-translational modification that regulates protein membrane association and protein−protein interaction (PPI).[13] Palmitoylation can influence protein localization, transportation, stability, and interactions.[14] Therefore, it is essential in several cellular processes, including signal transduction, metabolism, apoptosis, and disease development, including tumorigenesis. PD-L1 palmitoylation inhibition reduces PD-L1 expression in tumor cells, boosting T-cell immunity against the tumors.[15] A STAT3 palmitoylation cycle promotes TH17 differentiation and colitis.[16] Targeting NLRP3 palmitoylation has been proposed as a potential therapeutic approach for NLRP3 inflammasome-driven diseases. The DHHC family of palmitoyltransferases initiates palmitoylation, which can be reversed by several acyl protein thioesterases.[17]

Received: October 13, 2024
Revised: December 9, 2024
Accepted: December 20, 2024
Published: December 31, 2024

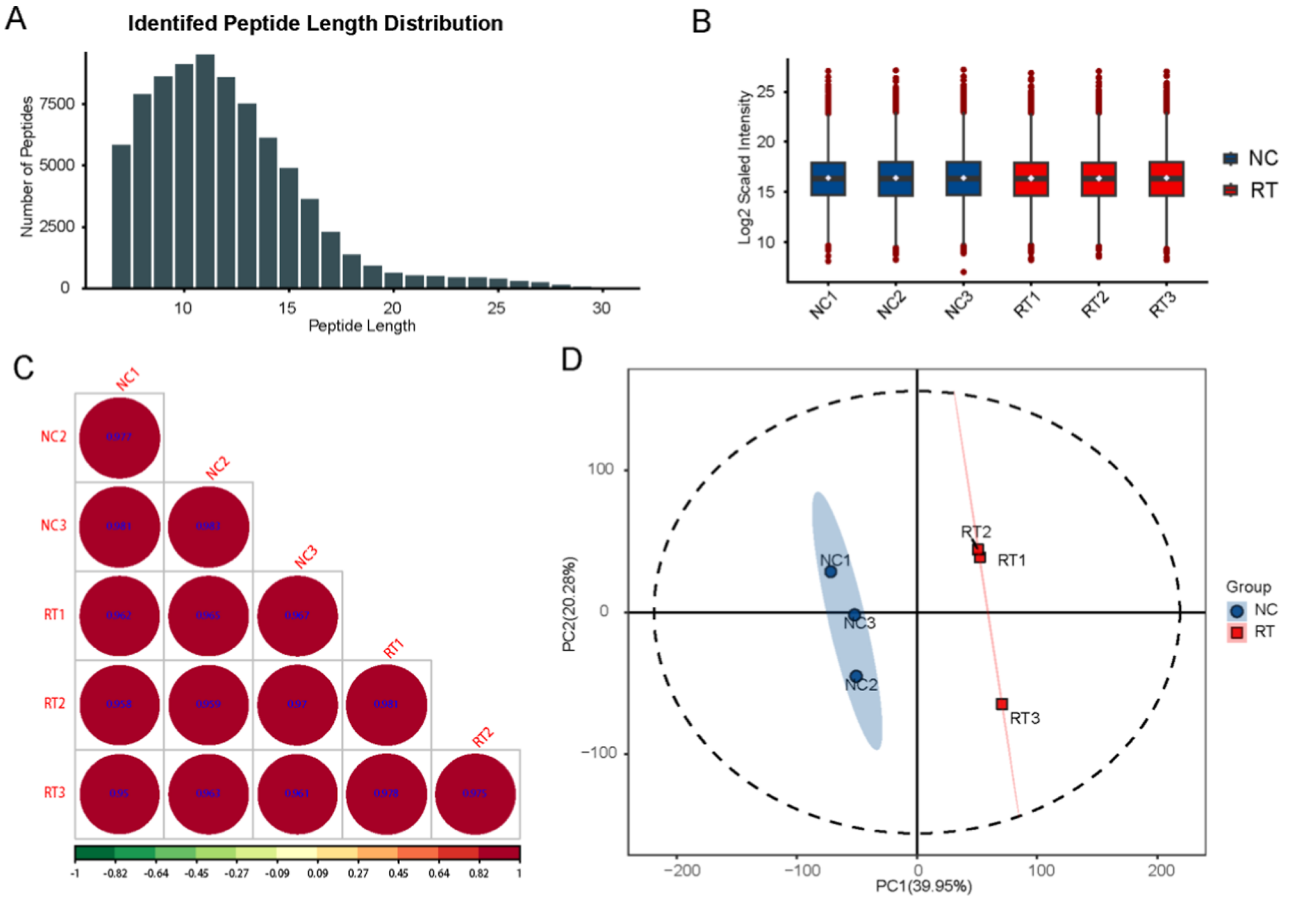

Figure 1. Quality control of samples. (A) Peptide length distribution of the identified peptides. (B) Boxplot of sample expression distribution. (C) Sample correlation plots (bubble plots). (D) Sample PCA score plot.

DHHC9-mediated GLUT1 S-palmitoylation promotes glioblastoma glycolysis and tumorigenesis.[18]

RT resistance is associated with several biological alterations within the tumor and in the surrounding environment.[4] Studies on the RT sensitivity in EC to palmitoylation are inconclusive. This study sequenced the proteome and protein palmitoylation of EC cells between RT and negative control (NC) to identify therapeutic targets for EC. This study aimed to clarify EC radioresistance by examining altered palmitoylation and identify new therapeutic targets by studying new ideas for EC treatment.

METHODS

Cell Line and Cell Culture. The EC cell line KYSE410 (RRID: CVCL_1352) was procured and characterized using short tandem repeat markers from Meixuan Company (Shanghai, China). Mycoplasma-free cells were used to perform all experiments. The cell lines were cultured in RPMI-1640 medium (HyClone; Cytiva) supplemented with 10% fetal bovine serum (FBS; FSP500; ExCell Bio, Uruguay), 100 U/mL penicillin, and 100 μg/mL streptomycin (Cat. #15140112, Gibco, Grand Island, NY, USA), and incubated at 37 °C in a 5% CO_2/95% air atmosphere. The RT group received an 8 Gy dose of superficial 6 MV photon irradiation within 5 min.

Sample Preparation. SDT lysis buffer containing 4% SDS, 100 mM DTT (Dithiothreitol, Sigma, D0632), and 100 mM Tris-HCl pH 8.0 was used to extract protein from the cells. The samples were subsequently boiled for 3 min and subjected to ultrasonication. Undissolved cellular debris was removed through centrifugation at 16,000*g* for 15 min. A BCA protein assay kit (BeyoTime China) was used to collect and quantify the resulting supernatant.

PROTEIN DIGESTION

The FASP (Filter-Aided Sample Preparation) method outlined by Wisniewski et al. was used for protein digestion.[19] A solution containing detergent, DTT, and IAA (Indole-3-acetic acid) in Urea Lysis buffer was used to inhibit reduced cysteine residues. Subsequently, the protein suspension was enzymatically digested with trypsin (Promega) at a 50:1 ratio overnight at 37 °C. The resulting peptide mixtures were isolated using centrifugation at 16,000 *g* for 15 min and purified using a C18 Stage Tip for subsequent liquid chromatography−mass spectrometry (LC−MS). The concentrations of reconstituted peptides were quantified using an OD280 measurement on a Nanodrop One device (Thermo, USA).

LC−MS/MS for Data-Independent Acquisition (DIA). The Vanquish chromatography system (Thermo Scientific) was used in proteomics assays for chromatographic separations. The buffer used in this study comprised solution A, containing 0.1% formic acid, and solution B, containing 0.1% formic acid in acetonitrile (85% acetonitrile composition). An Orbitrap Astral mass spectrometer (Thermo Scientific) was used for data-independent acquisition (DIA) mass spectrometry. Subsequently, DIA-NN software (version 1.8.1)[20,21] was used to integrate all mass spectrometry data to analyze the search library and construct a spectral database.

https://doi.org/10.1021/acsomega.4c09353
ACS Omega 2025, 10, 1541−1550

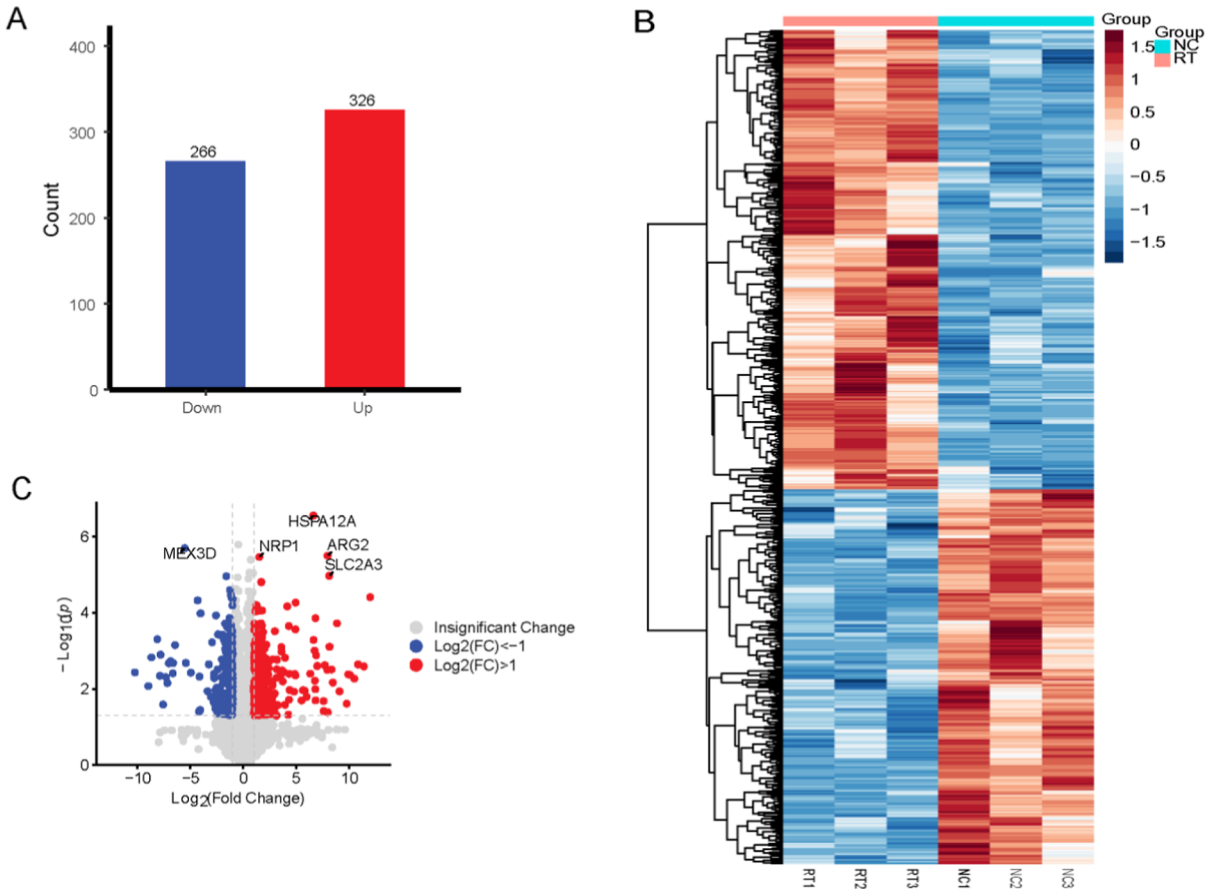

Figure 2. Differential proteins before and after RT. (A) Number of differential proteins. (B) Heatmap of the differential proteins. (C) Volcano map of differential proteins.

Sequence Database Searching. Mass spectrometry data were queried against the UniProtKB reviewed (Swiss-prot) database (UniProt-*Homo sapiens* (Human) [9606]-20240102.fasta) with trypsin as the digestion enzyme. Cysteine carbamidomethylation was designated a fixed modification, while acetylation of protein N-terminal residues and methionine oxidation were considered variable modifications for database searches. Each peptide could have up to one variable modification. Peptide lengths were limited to 7−30 amino acids, and peptide charges ranged from 1 to 4. Fragment ion m/z values ranged from 150−2000. The database search results were filtered and exported with <1% false discovery rate (FDR) at peptide-spectrum-matched and protein levels, respectively. Differentially expressed proteins (DEPs) were defined as those with a $P < 0.05$ and an absolute value of log fold change (LogFC) > 2.

Database Searching and Analysis for S-Palmitoylation Proteins. Spectronaut software (version 18; Biognosys AG, Switzerland) was used to analyze the DIA MS data. Tryptic cleavage specificity, variable methionine oxidation (M), variable protein N-terminal acetylation, variable *N*-ethylmaleimide (C), and carbamidomethylation (C) were used to analyze the MS data against the UniProtKB reviewed (Swiss-prot) database (uniprotkb_*H. sapiens* (Human)[9606]-204141_2024_03_26.fasta). A minimum of six amino acids per peptide and at least one unique peptide per protein were required for identification. An FDR of 1% was established for peptide and protein identification. According to the algorithm, site quantitation analysis was restricted to carbamidomethylated cysteine sites that were confidently localized with a site probability of ≥0.75. Intensity determination was used to perform label-free quantification. The median ratio was used to weigh and normalize the quantitative site ratios. A *t*-test was used to analyze the significant differences between RT and NC samples. The S-palmitoylation proteins that were differently detected between RT and NC were selected based on logFC > 3.0 and $P < 0.05$.

Bioinformatics Analysis. Microsoft Excel and R statistical computing software were used to perform bioinformatic analysis. The statistical language R was used to perform hierarchical clustering analysis and generate volcano plots. Data were extracted from UniProtKB/Swiss-Prot, the KEGG (https://www.genome.jp/kegg/), and Gene Ontology (GO) (https://geneontology.org/) to perform sequence annotation. Fisher's exact test was used to perform enrichment analyses for GO and KEGG with FDR correction for multiple tests. The GO terms were divided into biological process (BP), molecular function (MF), and cellular component (CC). The enriched GO and KEGG pathways demonstrated nominal statistical significance with $P < 0.01$ based on the Fisher exact test. Additionally, the STRING database and Cytoscape software were used to construct PPI networks. MoMo (http://meme-suite.org/tools/momo) was used to analyze the motif characteristics of the modification sites.

RESULTS

Quality Control of All Samples. This study used a ± 10 ppm threshold for peptide mass error and an FDR threshold of

https://doi.org/10.1021/acsomega.4c09353
ACS Omega 2025, 10, 1541−1550

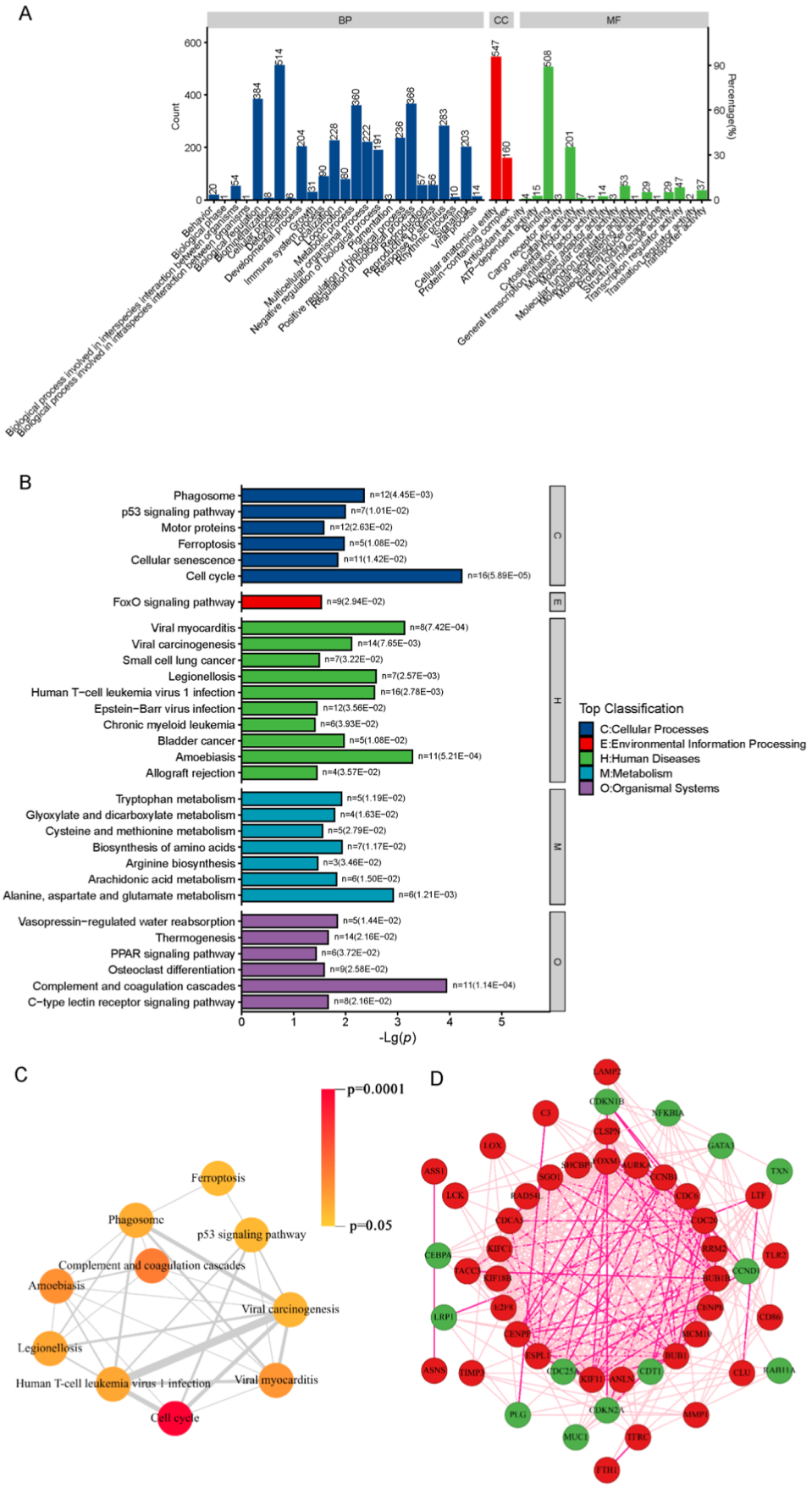

Figure 3. GO functional classifications. (A) Enrichment of KEGG pathway. (B) PPI network. (C,D) Analysis of differential proteins.

https://doi.org/10.1021/acsomega.4c09353
ACS Omega 2025, 10, 1541−1550

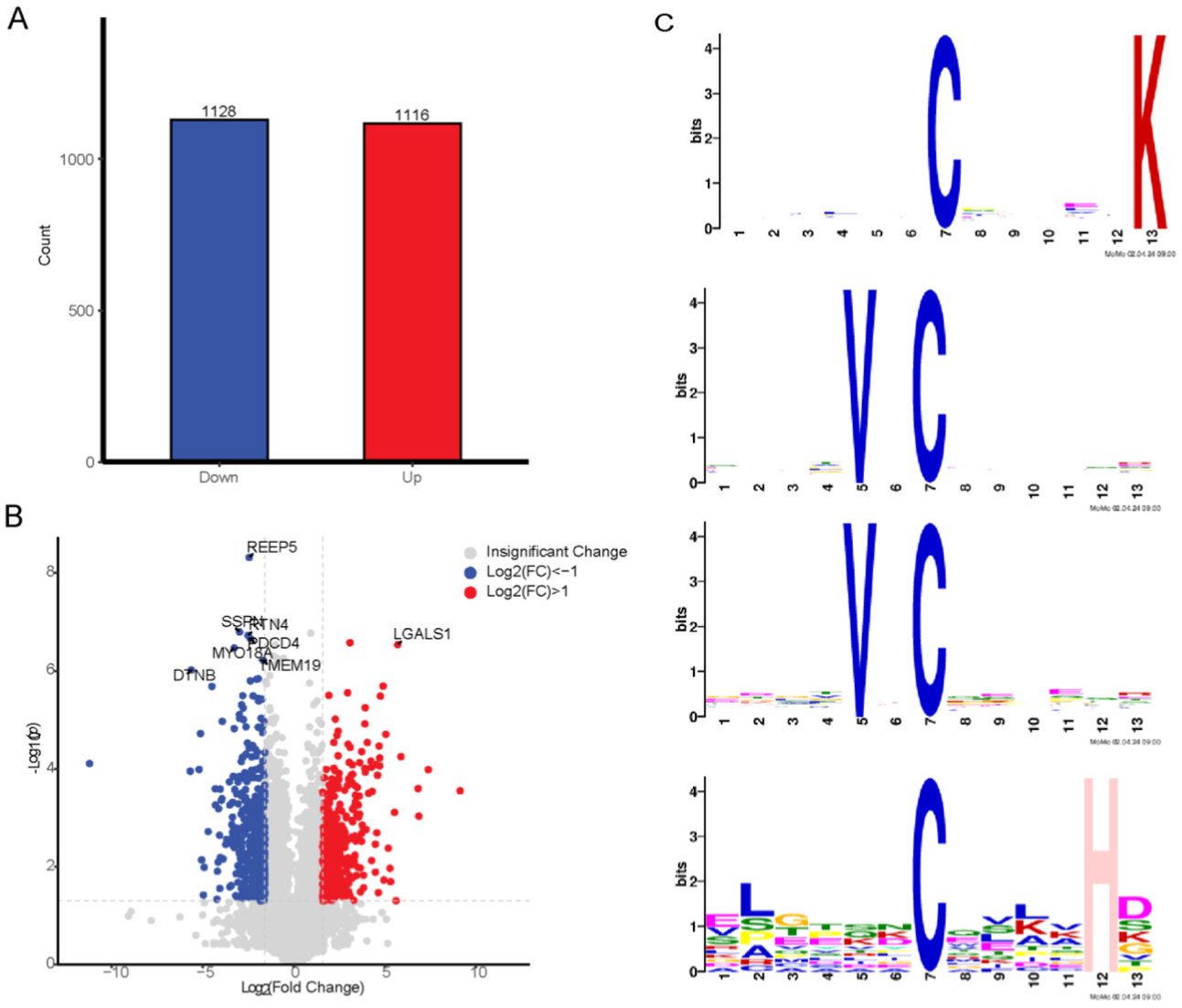

Figure 4. Differential S-palmitoylation proteins before and after RT. (A) Number of differential S-palmitoylation proteins. (B) Volcano map of differential S-palmitoylation proteins. (C) Sequence motif logos indicating the S-palmitoylation sites detected in proteins and the composition of position-specific amino acids surrounding the S-palmitoylation sites.

≤0.01 and ≤0.01 for library characterization as the screening criteria. Figure 1A depicts the distribution of peptides. Correlation and principal component analyses (PCA) were used to analyze expression distribution based on the protein expression in different samples. Figure 1B illustrates the expression distribution of the samples. The median number of samples in the same group was approximately at the same level, indicating superior data quality and good reproducibility. The correlation coefficient among samples in the same group was good (Figure 1C). The PCA score plot of samples (Figure 1D) indicates a high similarity among samples in the same group.

GO Functional Annotation and KEGG Pathway of all Proteins. The data set of all proteins was used to examine the GO functional annotation of CCs, BPs, and MFs (Figure S1A). All proteins were primarily found in cellular processes, cellular anatomical entities, and binding activities. These proteins participate in cellular biological processes. Figure S1B depicts the enriched KEGG pathway for all proteins. The top cellular processes identified were endocytosis, cell cycle, and autophagy. Protein processing in the endoplasmic reticulum and nucleocytoplasmic transport were identified as the significant KEGG pathways for genetic information processing. The KEGG pathway enrichment involved in environmental information processing was the phosphatidylinositol signaling system.

DEPs between RT and NC. LC−MS was used to identify 592 proteins in the RT groups, including 326 upregulation proteins and 266 downregulation proteins (Figure 2A and 2B). The top 20 upregulated and downregulated DEPs between RT and NC are presented in Tables S1 and S2. Figure 2C depicts the heatmap of RT and NC Kyse410 cells in triplicate. MEX3D (Mex-3 RNA Binding Family Member D) was significantly lower in RT, while heat shock protein A12A (HSPA12A), neuropilin-1 (NRP1), arginase 2 (ARG2), and SLC2A3 were significantly higher during RT.

The DEPs were primarily found in cellular processes, cellular anatomical entities, and binding activities (Figure 3A). These DEPs participated in cellular biological processes. This is identical to the GO functional annotation of all proteins. Figure 3B depicts the enriched KEGG pathway for DEPs. The primary cellular processes identified were the cell cycle and phagosome. The significant KEGG pathways for environment

https://doi.org/10.1021/acsomega.4c09353
ACS Omega 2025, 10, 1541−1550

Table 1. Top 20 Upregulation of Differential S-Palmitoylation Proteins before and after RT

accession	gene	protein name	Log2FC
A0A384MR27	LGALS1	galectin-1	5.71
B3KY36	MBLAC2	acyl-coenzyme A thioesterase MBLAC2	4.91
K7EQS7	KDSR	3-ketodihydrosphingosine reductase	2.96
Q92614	MYO18A	unconventional myosin-XVIIIa	1.93
Q96FV9	THOC1	THO complex subunit 1	4.76
P07602	PSAP	prosaposin	3.92
A0A0Y0BS51		CUB domain-containing protein 1	2.29
Q8TCG1	CIP2A	protein CIP2A	3.91
Q13501	SQSTM1	sequestosome-1	2.44
B4DRS4	HTATSF1	highly similar to Homo sapiens HIV TAT specific factor 1	5.06
Q9UI12	ATP6 V1H	V-type proton ATPase subunit H	2.38
A0A1B0GVV3	RILPL1	RILP-like protein 1	2.21
P52209	PGD	6-phosphogluconate dehydrogenase	4.04
Q9Y584	TIMM22	mitochondrial import inner membrane translocase subunit Tim22	2.99
B5MDF5	RAN	GTP-binding nuclear protein Ran	4.69
B3KNC3		nucleolar complex protein 2 homologue	3.10
A0A384MTS3	BCAR3	breast cancer antiestrogen resistance protein 3	3.73
A0A024QYR8	TM9SF2	transmembrane 9 superfamily member 2	2.44
A0A994J5B1	EPB41L2	erythrocyte membrane protein band 4.1 like 2	5.88
A0A1 × 7SBZ2	DDX17	probable ATP-dependent RNA helicase DDX17	4.72

Table 2. Top 20 Downregulation of Differential S-Palmitoylation Proteins before and after RT

accession	gene	protein name	Log2FC
B2R6C4	REEP5	receptor expression-enhancing protein 5	−2.45
B2RAU1	SSPN	sarcospan	−2.97
Q9NQC3	RTN4	reticulon-4	−2.50
B2R6E2	PDCD4	programmed cell death protein 4	−2.39
Q92614	MYO18A	unconventional myosin-XVIIIa	−3.27
Q96HH6	TMEM19	transmembrane protein 19	−1.68
B7Z6A9	DTNB	dystrobrevin	−5.62
P19075	TSPAN8	tetraspanin-8; tetraspanin	−1.95
Q53HA8	MCOLN1	mucolipin-1	−2.04
A0A2U3TZN6	CASK	calcium/calmodulin-dependent serine protein kinase	−2.39
C9JJX6	ARVCF	splicing regulator ARVCF	−4.49
Q99959	PKP2	plakophilin-2	−2.80
P63096	GNAI1	guanine nucleotide-binding protein G(i) subunit alpha-1	−2.24
Q96EX2	RNFT2	E3 ubiquitin-protein ligase RNFT2	−1.94
Q9Y2G3	ATP11B	phospholipid-transporting ATPase IF	−1.75
O60502	OGA	protein *O*-GlcNAcase	−1.93
B2R8C2	FRK	tyrosine-protein kinase	−2.87
Q9BRT2	UQCC2	ubiquinol-cytochrome c reductase complex assembly factor 2	−2.77
Q96EX2	RNFT2	E3 ubiquitin-protein ligase RNFT2	−2.98
D6RJC3	INPP4B	phosphatidylinositol-3,4-bisphosphate 4-phosphatase	−1.79

information processing were identified as the Forkhead box O (FoxO) signaling pathway. Enriching KEGG pathways involved in metabolism included alanine, aspartate, and glutamate metabolism. We combined PPI relationships from the STRING database and pathway-protein relationships into one network. Coincidentally, those significant pathways were found in PPI. Coexpressed protein clusters were found to be associated with ferroptosis, phagosome, cell cycle, p53 signaling pathway, amoebiasis, viral myocarditis, viral carcinogenesis, legionellosis, human T-cell leukemia virus 1 infection, complement and coagulation cascades (Figure 3C). Additionally, a PageRank algorithm was used to select the top 50 vertices for the network (Figure 3D).

GO Functional Annotation and KEGG Pathway of S-Palmitoylation Proteins. The GO functional annotation of S-palmitoylation proteins was primarily found in cellular processes, cellular anatomical entities, and binding activities (Figure S2A). Coincidentally, the GO functional annotations were consistent across all proteins. Figure S2B depicts the enriched KEGG pathway for S-palmitoylation protein. The cell cycle was illustrated as the most essential cellular process. Protein processing in nucleocytoplasmic transport is a significant KEGG pathway for genetic information processing. The phosphatidylinositol signaling system was the most enriched KEGG pathway in environmental information processing.

Identification and Quantification of S-Palmitoylation Protein. S-palmitoylation sequencing identified 1729 cysteine sites with S-palmitoylation modification in the kyse 410 cell line between RT and NC. Moreover, 830 S-palmitoylation cysteine sites were upregulated, and 899 S-palmitoylation cysteine sites were downregulated (Figure 4A). Figure 4B

https://doi.org/10.1021/acsomega.4c09353
ACS Omega 2025, 10, 1541−1550

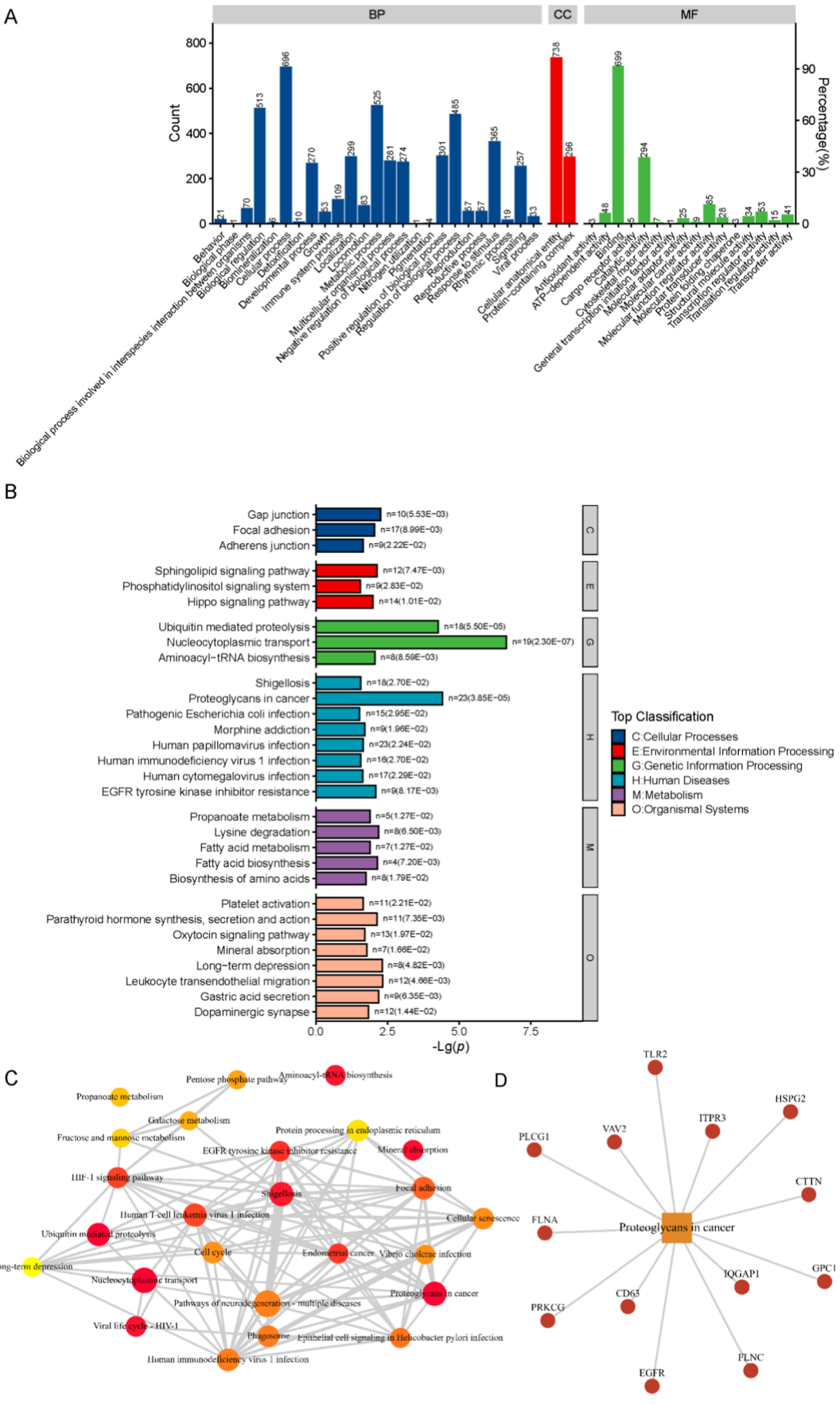

Figure 5. GO functional classifications. (A) Enrichment of KEGG pathway. (B) PPI network. (C,D) Analysis of differential S-palmitoylation proteins.

https://doi.org/10.1021/acsomega.4c09353
ACS Omega 2025, 10, 1541−1550

depicts a volcano plot of S-palmitoylation cysteine sites. S-palmitoylation modification of receptor accessory protein 5 (REEP5), sarcospan (SSPN), programmed cell death 4 (PDCD4), Myosin XVIII (AMYO18A), RTN4, TMEM19, DTNB (dystrobrevin beta), and other proteins were decreased, while S-palmitoylation modification of LGALS1 and other proteins was increased. There were 1729 S-palmitoylation modified Cys-sites in 1044 peptides, with 685 of them containing more than two Cys-sites. Tables 1 and 2 present the top 20 differential S-palmitoylation proteins and Cys-sites.

MoMo software and hierarchical cluster analysis were used to investigate the S-palmitoylated sites from six amino acids upstream to six amino acids downstream of the flanking sequences. The frequency of cysteine (C) residue at position 7 and lysine (K) residue at position 13 was the highest; valine (V) residue was highest at position 5, while cysteine (C) residue was highest at position 7. Among upregulation of S-palmitoylated sites, the frequency of C residue at position 7 and histidine (H) residue at position 12 was highest in upregulated S-palmitoylation. The horizontal coordinate indicates the position of the amino acid in the sequence window (base sequence of the modification site), while the vertical coordinate indicates the relative frequency of amino acids appearing at each site (Figure 4C).

GO Functional Annotation and KEGG Pathway of Differential S-Palmitoylation Proteins. The GO functional annotation of S-palmitoylation proteins was primarily found in cellular processes, cellular anatomical entities, and binding activities (Figure 5A). Coincidentally, the GO functional annotations were consistent across all proteins and the S-palmitoylation protein. Figure 5B depicts an enriched KEGG pathway for differential S-palmitoylation proteins. The top cellular processes were gap junction and focal adhesion. The phosphatidylinositol signaling system was the most enriched KEGG pathway involved in environmental information processing. Protein processing in nucleocytoplasmic transport is a significant KEGG pathway for genetic information processing. Coincidentally, those significant pathways were found in PPI. Several coexpressed protein clusters were identified, including proteoglycans in cancer, shigellosis, EGFR tyrosine kinase inhibitor resistance, nucleocytoplasmic transport, and mineral absorption (Figure 5C). Toll-like receptor (TLR) 2, Inositol 1,4,5-triphosphate receptor family (ITPRs), Heparan sulfate proteoglycan 2 (HSPG2), cortactin (CTTN), glypican-1 (GPC1), IQ motif-containing GTPase-activating protein 1 (IQGAP1), filamin C (FLNC), EGFR, CD63, protein kinase C gamma (PRKCG), filamin A (FLNA), phospholipase C gamma 1 (PLCG 1) and vav guanine nucleotide exchange factor 2 (VAV2) were associated with proteoglycans in cancer (Figure 5D).

DISCUSSION

RT is an important treatment option for patients with EC. In the past decade, genomic and transcriptomic studies have helped to understand the molecular mechanisms of EC. However, molecular typing, prognostic markers, and targeted therapeutic targets of EC based on genomic and transcriptomic data remain relatively limited compared to other cancer types. Proteomics and protein modification analysis reveal tumor biological codes that remain inscrutable through genome and transcriptome at a deeper level, thereby paving a new direction for cancer clinical treatment research. This study examined the potential mechanisms by investigating the differences in proteomics and protein modification proteomics of EC cells before and after RT.

This study identified 266 downregulation proteins. MEX3D was significantly lower in EC cells after RT. MEX3D has recently been found to exhibit oncogenic properties in various cancer types.[22] Besides, HSPA12A, NRP1, ARG2, and SLC2A3 were significantly higher in RT. These proteins have been previously reported in the literature. Hepatocyte HSPA12A inhibits macrophage chemotaxis and activation, reducing liver ischemia/reperfusion injury.[23] NRP1 enhances EC progression by promoting P65-dependent cell proliferation.[24] ARG is a key hydrolase in the urea cycle, and ARG2 was aberrantly upregulated in various cancer types. It played crucial roles in the regulation of tumor growth and metastasis through multiple mechanisms, including regulating L-arginine metabolism and influencing the tumor immune microenvironment.[25] SLC2A3 knockdown inhibited cell proliferation and migration in head and neck squamous cell carcinoma, indicating that it is an oncogene.[26] These differences in protein levels before and after RT suggest that RT regulation activates tumor suppressor proteins and decreases oncogenic proteins. Several factors may influence this deregulation. A previous study reported that RT significantly affects the cellular composition of the EC immune microenvironment.[27]

We performed GO pathway analyses, and the deregulated proteins were primarily found in cellular processes, cellular anatomical entities, and binding activities. Numerous proteins were differentially expressed in EC, including significant upregulation of the cell cycle, DNA repair, immune response, and EMT-related proteins, and downregulation of proteins involved in metabolism and estrogen response-related pathways.[28] The results varied because we studied different specimens.

The cell cycle and phagosome were identified as the most important cellular processes of differential proteins. Cell cycle arrest is one of the causes of cancer resistance to RT therapy.[29] Phagosomes are highly dynamic organelles formed by macrophages and phagocytic innate immune cells.[30] Autophagy is among the most essential cellular processes for all proteins. Autophagy is a fundamental factor in tumor survival during radiotherapeutic stress.[31] FoxO signaling pathway was identified in KEGG. The FOXO plays a pivotal functional role as a tumor suppressor in various cancers.[32] Additionally, this pathway was found in the KEGG pathway in mice with RT lung injury.[33] KEGG enrichment pathways related to metabolism included alanine, aspartate, and glutamate metabolisms. The metabolic landscape of gastric cancer revealed that alanine, aspartate, and glutamate metabolisms were significantly associated with gastric cancer prevalence and progression.[34] PPI revealed and explained the ferroptosis, complement, and coagulation cascades. Radiotherapy induces ferroptosis in patients with cancer, and increased ferroptosis correlates with better response and prolonged survival after radiotherapy in patients with cancer,[35] whereas the complement and coagulation cascade pathways are potential biomarkers for chemotherapy resistance and survival in patients with soft tissue sarcoma.[36]

This study investigated the underlying mechanism of RT through S-palmitoylation modification in EC cells. We found that 830 S-palmitoylation cysteine sites were upregulated, while 899 S-palmitoylation cysteine sites were downregulated. S-palmitoylation modifiction of REEP5, SSPN, PDCD4, MYO18A, RTN4, TMEM19, and DTNB were decreased.

https://doi.org/10.1021/acsomega.4c09353
ACS Omega 2025, 10, 1541−1550

REEP5 depletion causes vacuolization of the sarco-endoplasmic reticulum and defects in cardiac function.[37] SSPN overexpression improves skeletal, pulmonary, and cardiac performance at the sarcolemma.[38] *PDCD4* is a tumor suppressor gene that regulates cell apoptosis, transformation, invasion, and tumor progression.[39] DNA damage causes the Golgi apparatus to disperse, which requires the involvement of GOLPH3, MYO18A, F-actin, and the DNA damage protein kinase.[40] RTN4 knockdown impedes cancer cell proliferation in vitro and in mice tumor xenografts.[41]

The top cellular processes were gap junction and focal adhesion. Gap junctions are essential for coordinating multicellular behavior.[42] Focal adhesions are specialized sites where cells attach to the extracellular matrix.[43] The phosphatidylinositol signaling system was the most enriched KEGG pathway in environmental information processing. RT activates phosphatidylinositol 3-kinase and AKT signaling pathways.[44] Protein processing in nucleocytoplasmic transport is a significant KEGG pathway for genetic information processing. Nucleocytoplasmic transport regulates protein levels and activity in the nucleus or cytoplasm.[45] PPI identified proteoglycans in cancer and EGFR tyrosine kinase inhibitor resistance. Proteoglycans are the main components of the extracellular matrix. They interact with other proteins, soluble bioactive molecules, the surrounding matrix, cell surface receptors, and enzymes, allowing cancer cells to invade and metastasize.[46] These proteins are associated with the EGFR tyrosine kinase inhibitor resistance pathway, suggesting that potential therapeutic target genes may be contained for EGFR tyrosine kinase inhibitor resistance. TLR2, ITPR3, HSPG2, CTTN, GPC1, IQGAP1, FLNC, EGFR, CD63, PRKCG, FLNA, PLCG1, and VAV2 were involved in cancer related proteoglycan interactions. The mechanism of palmitoylation of these proteins in roteoglycans in cancer requires further investigation.

CONCLUSION

This study demonstrated that RT significantly affects protein expression and S-palmitoylation levels in EC cell lines. Furthermore, RT affects cancer-related cellular processes and pathways. These findings enhance the understanding of the molecular mechanisms underlying the response of EC cells to RT treatment.

ASSOCIATED CONTENT

Data Availability Statement

The mass spectrometry proteomics data have been deposited to the ProteomeXchange Consortium via the PRIDE partner repository.

Supporting Information

The Supporting Information is available free of charge at https://pubs.acs.org/doi/10.1021/acsomega.4c09353.

Figure S1. GO functional classifications. (A) Enrichment of KEGG pathway. (B) Analysis of all proteins. Figure S2. GO functional classifications. (A) Enrichment of KEGG pathway. (B) Analysis of all S-palmitoylation proteins. Table S1.The top 20 up-regulation of DEPs between before and after radiation. Table S2. The top 20 down-regulation of DEPs between before and after radiation (PDF)

AUTHOR INFORMATION

Corresponding Authors

Chi Pan − *Department of General Surgery, The Affiliated Taizhou People's Hospital of Nanjing Medical University, Taizhou School of Clinical Medicine, Nanjing Medical University, Taizhou 225300, China*; orcid.org/0000-0001-5558-6393; Phone: +86 15005268235; Email: panchi@njmu.edu.cn

Gaohua Han − *Department of Oncology, The Affiliated Taizhou People's Hospital of Nanjing Medical University, Taizhou School of Clinical Medicine, Nanjing Medical University, Taizhou 225300, China*; Phone: +86 13852613099; Email: danny_75@njmu.edu.cn

Author

Qingtao Ni − *Department of Oncology, The Affiliated Taizhou People's Hospital of Nanjing Medical University, Taizhou School of Clinical Medicine, Nanjing Medical University, Taizhou 225300, China*

Complete contact information is available at: https://pubs.acs.org/10.1021/acsomega.4c09353

Author Contributions

All authors contributed to the study's conception and design. Q.N. performed the experimental operation and collected the data. C.P. and G.H. designed the experiment and analyzed the data. Q.N. wrote the first draft of the manuscript, and all authors commented on previous versions. All authors read and approved the final manuscript.

Funding

This work was supported by National Natural Youth Incubation Program, Taizhou School of Clinical Medicine, Nanjing Medical University (no. TZKY20220109).

Notes

The authors declare no competing financial interest.
The author reports no conflicts of interest in this work.

REFERENCES

(1) Siegel, R. L.; Giaquinto, A. N.; Jemal, A. Cancer statistics, 2024. *J. CA Cancer J. Clin* **2024**, *74* (1), 12−49.
(2) Zhu, H.; Ma, X.; Ye, T.; et al. Esophageal cancer in China: Practice and research in the new era. *J. Int. J. Cancer* **2023**, *152* (9), 1741−1751.
(3) Wang, F.; Zhang, L.; Xu, Y.; et al. Comprehensive Analysis and Identification of Key Driver Genes for Distinguishing Between Esophageal Adenocarcinoma and Squamous Cell Carcinoma. *J. Front Cell Dev Biol.* **2021**, *9*, 676156.
(4) Buckley, A. M.; Lynam-Lennon, N.; O'Neill, H.; et al. Targeting hallmarks of cancer to enhance radiosensitivity in gastrointestinal cancers. *J. Nat. Rev. Gastroenterol Hepatol* **2020**, *17* (5), 298−313.
(5) de Groot, C.; Beukema, J. C.; Langendijk, J. A.; et al. Radiation-Induced Myocardial Fibrosis in Long-Term Esophageal Cancer Survivors. *J. Int. J. Radiat Oncol Biol. Phys.* **2021**, *110* (4), 1013−1021.
(6) Li, M.-Y.; Fan, L. N.; Han, D. H.; et al. Ribosomal S6 protein kinase 4 promotes radioresistance in esophageal squamous cell carcinoma. *J. J. Clin Invest* **2020**, *130* (8), 4301−4319.
(7) Belli, M.; Tabocchini, M. A. Ionizing Radiation-Induced Epigenetic Modifications and Their Relevance to Radiation Protection. *J. Int. J. Mol. Sci.* **2020**, *21* (17), 5993.
(8) Guan, H.; Wang, P.; Zhang, P.; et al. Diverse modes of H3K36me3-guided nucleosomal deacetylation by Rpd3S. *J. Nature* **2023**, *620* (7974), 669−675.

(9) Liao, L.; He, Y.; Li, S. J.; et al. Lysine 2-hydroxyisobutyrylation of NAT10 promotes cancer metastasis in an ac4C-dependent manner. *J. Cell Res.* **2023**, *33* (5), 355−371.
(10) Caspa Gokulan, R.; Paulrasu, K.; Azfar, J.; et al. Protein adduction causes non-mutational inhibition of p53 tumor suppressor. *Cell Rep.* **2023**, *42* (1), 112024.
(11) Chen, B.; Sun, Y.; Niu, J.; et al. Protein Lipidation in Cell Signaling and Diseases: Function, Regulation, and Therapeutic Opportunities. *J. Cell Chem. Biol.* **2018**, *25* (7), 817−831.
(12) Aicart-Ramos, C.; Valero, R. A.; Rodriguez-Crespo, I. Protein palmitoylation and subcellular trafficking. *J. Biochim Biophys Acta* **2011**, *1808* (12), 2981−2994.
(13) Jiang, H.; Zhang, X.; Chen, X.; et al. Protein Lipidation: Occurrence, Mechanisms, Biological Functions, and Enabling Technologies. *J. Chem. Rev.* **2018**, *118* (3), 919−988.
(14) Fan, Z.; Hao, Y.; Huo, Y.; et al. Modulators for palmitoylation of proteins and small molecules. *J. Eur. J. Med. Chem.* **2024**, *271*, 116408.
(15) Yao, H.; Lan, J.; Li, C.; et al. Inhibiting PD-L1 palmitoylation enhances T-cell immune responses against tumours. *J. Nat. Biomed Eng.* **2019**, *3* (4), 306−317.
(16) Zhang, M.; Zhou, L.; Xu, Y.; et al. A STAT3 palmitoylation cycle promotes T(H)17 differentiation and colitis. *J. Nature* **2020**, *586* (7829), 434−439.
(17) Gu, M.; Jiang, H.; Tan, M.; Yu, L.; Xu, N.; Li, Y.; Wu, H.; Hou, Q.; Dai, C. Palmitoyltransferase DHHC9 and acyl protein thioesterase APT1 modulate renal fibrosis through regulating *β*-catenin palmitoylation. *J. Nat. Commun.* **2023**, *14* (1), 6682.
(18) Zhang, Z.; Li, X.; Yang, F.; Chen, C.; Liu, P.; Ren, Y.; Sun, P.; Wang, Z.; You, Y.; Zeng, Y. X.; et al. DHHC9-mediated GLUT1 S-palmitoylation promotes glioblastoma glycolysis and tumorigenesis. *J. Nat. Commun.* **2021**, *12* (1), 5872.
(19) Wisniewski, J. R.; Zougman, A.; Nagaraj, N.; et al. Universal sample preparation method for proteome analysis. *J. Nat. Methods* **2009**, *6* (5), 359−362.
(20) Demichev, V.; Messner, C. B.; Vernardis, S. I.; et al. DIA-NN: neural networks and interference correction enable deep proteome coverage in high throughput. *J. Nat. Methods* **2020**, *17* (1), 41−44.
(21) Barkovits, K.; Pacharra, S.; Pfeiffer, K.; et al. Reproducibility, Specificity and Accuracy of Relative Quantification Using Spectral Library-based Data-independent Acquisition. *J. Mol. Cell Proteomics* **2020**, *19* (1), 181−197.
(22) Zheng, Z.; Chen, X.; Cai, X.; Lin, H.; Xu, J.; Cheng, X. RNA-binding protein MEX3D promotes cervical carcinoma tumorigenesis by destabilizing TSC22D1 mRNA. *J. Cell Death Discov* **2022**, *8* (1), 250.
(23) Du, S.; Zhang, X.; Jia, Y.; et al. Hepatocyte HSPA12A inhibits macrophage chemotaxis and activation to attenuate liver ischemia/reperfusion injury via suppressing glycolysis-mediated HMGB1 lactylation and secretion of hepatocytes. *J. Theranostics* **2023**, *13* (11), 3856−3871.
(24) Shi, F.; Shang, L.; Yang, L. Y.; et al. Neuropilin-1 contributes to esophageal squamous cancer progression via promoting P65-dependent cell proliferation. *J. Oncogene* **2018**, *37* (7), 935−943.
(25) Niu, F.; Yu, Y.; Li, Z.; et al. Arginase: An emerging and promising therapeutic target for cancer treatment. *J. Biomed Pharmacother* **2022**, *149*, 112840.
(26) Chai, F.; Zhang, J.; Fu, T.; Jiang, P.; Huang, Y.; Wang, L.; Yan, S.; Yan, X.; Yu, L.; Xu, Z.; et al. Identification of SLC2A3 as a prognostic indicator correlated with the NF-*κ*B/EMT axis and immune response in head and neck squamous cell carcinoma. *J. Channels (Austin)* **2023**, *17* (1), 2208928.
(27) Han, D.; Han, Y.; Guo, W.; Wei, W.; Yang, S.; Xiang, J.; Che, J.; Zhu, L.; Hang, J.; van den Ende, T.; et al. High-dimensional single-cell proteomics analysis of esophageal squamous cell carcinoma reveals dynamic alterations of the tumor immune microenvironment after neoadjuvant therapy. *J. J. Immunother Cancer* **2023**, *11* (11), No. e007847.
(28) Liu, W.; Xie, L.; He, Y. H.; Wu, Z. Y.; Liu, L. X.; Bai, X. F.; Deng, D. X.; Xu, X. E.; Liao, L. D.; Lin, W.; et al. Large-scale and high-resolution mass spectrometry-based proteomics profiling defines molecular subtypes of esophageal cancer for therapeutic targeting. *J. Nat. Commun.* **2021**, *12* (1), 4961.
(29) Wu, Y.; Song, Y.; Wang, R.; Wang, T. Molecular mechanisms of tumor resistance to radiotherapy. *J. Mol. Cancer* **2023**, *22* (1), 96.
(30) Dean, P.; Heunis, T.; Hartlova, A.; et al. Regulation of phagosome functions by post-translational modifications: a new paradigm. *J. Curr. Opin Chem. Biol.* **2019**, *48*, 73−80.
(31) Zheng, W.; Chen, Q.; Liu, H.; et al. SDC1-dependent TGM2 determines radiosensitivity in glioblastoma by coordinating EPG5-mediated fusion of autophagosomes with lysosomes. *J. Autophagy* **2023**, *19* (3), 839−857.
(32) Farhan, M.; Wang, H.; Gaur, U.; et al. FOXO Signaling Pathways as Therapeutic Targets in Cancer. *J. Int. J. Biol. Sci.* **2017**, *13* (7), 815−827.
(33) Zhang, X. Z.; Chen, M. J.; Fan, P. M.; et al. Prediction of the Mechanism of Sodium Butyrate against Radiation-Induced Lung Injury in Non-Small Cell Lung Cancer Based on Network Pharmacology and Molecular Dynamic Simulations and Molecular Dynamic Simulations. *J. Front Oncol* **2022**, *12*, 809772.
(34) Yuan, Q.; Deng, D.; Pan, C.; et al. Integration of transcriptomics, proteomics, and metabolomics data to reveal HER2-associated metabolic heterogeneity in gastric cancer with response to immunotherapy and neoadjuvant chemotherapy. *J. Front Immunol* **2022**, *13*, 951137.
(35) Lei, G.; Zhang, Y.; Koppula, P.; et al. The role of ferroptosis in ionizing radiation-induced cell death and tumor suppression. *J. Cell Res.* **2020**, *30* (2), 146−162.
(36) Zhang, J.; Chen, M.; Zhao, Y.; et al. Complement and coagulation cascades pathway correlates with chemosensitivity and overall survival in patients with soft tissue sarcoma. *J. Eur. J. Pharmacol* **2020**, *879*, 173121.
(37) Lee, S. H.; Hadipour-Lakmehsari, S.; Murthy, H. R.; Gibb, N.; Miyake, T.; Teng, A. C. T.; Cosme, J.; Yu, J. C.; Moon, M.; Lim, S.; et al. REEP5 depletion causes sarco-endoplasmic reticulum vacuolization and cardiac functional defects. *J. Nat. Commun.* **2020**, *11* (1), 965.
(38) Parvatiyar, M. S.; Brownstein, A. J.; Kanashiro-Takeuchi, R. M.; et al. Stabilization of the cardiac sarcolemma by sarcospan rescues DMD-associated cardiomyopathy. *JCI Insight* **2019**, *5* (11), No. e123855.
(39) Cui, H.; Wang, Q.; Lei, Z.; Feng, M.; Zhao, Z.; Wang, Y.; Wei, G. DTL promotes cancer progression by PDCD4 ubiquitin-dependent degradation. *J. J. Exp Clin Cancer Res.* **2019**, *38* (1), 350.
(40) Farber-Katz, S. E.; Dippold, H. C.; Buschman, M. D.; et al. DNA damage triggers Golgi dispersal via DNA-PK and GOLPH3. *J. Cell* **2014**, *156* (3), 413−427.
(41) Pathak, G. P.; Shah, R.; Kennedy, B. E.; et al. RTN4 Knockdown Dysregulates the AKT Pathway, Destabilizes the Cytoskeleton, and Enhances Paclitaxel-Induced Cytotoxicity in Cancers. *J. Mol. Ther* **2018**, *26* (8), 2019−2033.
(42) Li, Y.; Liu, W.; Tang, Q.; et al. Gap-Junction-Dependent Labeling of Nascent Proteins in Multicellular Networks. *J. ACS Chem. Biol.* **2019**, *14* (2), 182−185.
(43) Zhu, Y.; Wu, Y.; Kim, J. I.; et al. Arf GTPase-activating protein AGAP2 regulates focal adhesion kinase activity and focal adhesion remodeling. *J. J. Biol. Chem.* **2009**, *284* (20), 13489−13496.
(44) Mardanshahi, A.; Gharibkandi, N. A.; Vaseghi, S.; et al. The PI3K/AKT/mTOR signaling pathway inhibitors enhance radiosensitivity in cancer cell lines. *J. Mol. Biol. Rep* **2021**, *48* (8), 1−14.
(45) Kelley, J. B.; Paschal, B. M. Fluorescence-based quantification of nucleocytoplasmic transport. *J. Methods* **2019**, *157*, 106−114.
(46) Zhu, Y.; Cheung, A. Proteoglycans and their functions in esophageal squamous cell carcinoma. *J. World J. Clin Oncol* **2021**, *12* (7), 507−521.

https://doi.org/10.1021/acsomega.4c09353
ACS Omega 2025, 10, 1541−1550